report

J Neurophysiol 90: 2777–2784, 2003;
10.1152/jn.00231.2003.

Static Ocular Counterroll Is Implemented Through the 3-D Neural Integrator

J. Douglas Crawford,[1–3] Douglas B. Tweed,[1,2,4] and Tutis Vilis[1,5]

[1]*Canadian Institutes for Health Research Group for Action and Perception and* [2]*Centre for Vision Research, and* [3]*Departments of Psychology, Biology, Kinesiology and Health Sciences, York University, Toronto, Ontario M3J 1P3, Canada;* [4]*Departments of Physiology and Medicine, University of Toronto, Toronto, Ontario M5S 1A8, Canada; and* [5]*Departments of Physiology and Ophthalmology, University of Western Ontario, London, Ontario N6A 5C1, Canada*

Submitted 11 March 2003; accepted in final form 8 June 2003

Crawford, J. Douglas, Douglas B. Tweed, and Tutis Vilis. Static ocular counterroll is implemented through the 3-D neural integrator. *J Neurophysiol* 90: 2777–2784, 2003; 10.1152/jn.00231.2003. Static head roll about the naso-occipital axis is known to produce an opposite ocular counterroll with a gain of approximately 10%, but the purpose and neural mechanism of this response remain obscure. In theory counterroll could be maintained either by direct tonic vestibular inputs to motoneurons, or by a neurally integrated pulse, as observed in the saccade generator and vestibulo-ocular reflex. When simulated together with ocular drift related to torsional integrator failure, the direct tonic input model predicted that the pattern of drift would shift torsionally as in ordinary counterroll, but the integrated pulse model predicted that the equilibrium position of torsional drift would be unaffected by head roll. This was tested experimentally by measuring ocular counterroll in 2 monkeys after injection of muscimol into the mesencephalic interstitial nucleus of Cajal. Whereas 90° head roll produced a mean ocular counterroll of 8.5° (±0.7° SE) in control experiments, the torsional equilibrium position observed during integrator failure failed to counterroll, showing a torsional shift of only 0.3° (±0.6° SE). This result contradicted the direct tonic input model, but was consistent with models that implement counterroll by a neurally integrated pulse.

INTRODUCTION

When the head is stationary in a rolled position—for example, with the right ear tilted toward the right shoulder—the eye shows a sustained *counterroll*, tilting torsionally in the opposite direction but only about 6–10% as far (Baarsma and Collewijn 1975; Collewijn et al. 1985; Ott 1992; Seidman et al. 1995). The gain of this response is thus substantially lower than that of the dynamic torsional responses observed *during* head rotation (Collewijn et al. 1985). However, in contrast to the latter, static ocular counterroll is sustained indefinitely across saccadic eye movements, resulting in a constant torsional shift in the 3-D range of eye positions (Crawford and Vilis 1991; Haslwanter et al. 1992). Despite many recent studies on the vestibular control of eye roll (Angelaki and Hess 1999; Bockisch and Haslwanter 2001; Furman and Schor 2003; Hess and Angelaki 1997b,c, 1999; Kori et al. 2001; Misslisch et al. 2001; Paige and Tomko 1991; Telford et al. 1997), the purpose and neural mechanism of static ocular counterroll remain obscure.

The sensory drive for counterroll comes from the otolith organs, which sense head tilt (Schor et al. 1984; Tomko et al. 1981). But how do the otolith signals reach the eye muscles? One possibility is the direct route. Otolith afferents project, by the vestibular nuclei, to the extraocular motoneurons, so the commands for counterroll could reach the eyes by this path. According to this view, when the head is tilted clockwise (CW), excited otolith afferents tonically activate muscles that hold the eyes counterclockwise (CCW). This *direct tonic* theory of counterroll was the most popular over the last two decades (e.g., Glasauer et al. 1998). However, this scheme is difficult to reconcile with the polysynaptic connections between the otolith organs and the motoneurons that control ocular counterrroll (Sasaki et al. 1991; Uchino et al. 1996). Here we present evidence for another view more consistent with this anatomy: counterroll, like every other known conjugate eye-movement system, acts through a structure known as the *oculomotor neural integrator*.

The integrator is a neural system that converts eye-velocity commands into signals that control eye position, including torsional eye position (Crawford and Vilis 1993; Fukushima et al.1992; Helmchen et al.1998). An appropriate pulse of input to the integrator could be the cause of sustained ocular counterroll (Crawford and Vilis 1991; Glasauer et al. 2001; Vilis 1993). Otolith afferents themselves do not code appropriate pulses, but it is likely—for reasons we will discuss later—that otolith signals influence other eye-movement systems that do pulse. One example is the saccadic system, which shifts the gaze line rapidly between objects of interest. Saccadic burst neurons emit pulses of firing that, passing through the oculomotor integrator, yield eye-position commands that hold the eye in its new orientation until the next saccade. Our suggestion, then, is that when the head tilts, say, CW, the otolith organs inform the saccadic system, causing it to alter its pulsatile output in such a way that the integrator now codes eye positions that are tilted slightly CCW. Here we test between this *integrated pulse* model and the *direct tonic* model of ocular counterroll, as reported previously in abstract form (Crawford and Vilis 1999).

Simulations and predictions

The purpose of this section is to develop a test that hinges on the basic difference between the integrated pulse model and

Address for reprint requests and other correspondence: J. D. Crawford, Department of Psychology, York University, 4700 Keele St., North York, Ontario M3J 1P3, Canada (E-mail: JDC@yorku.ca).

The costs of publication of this article were defrayed in part by the payment of page charges. The article must therefore be hereby marked "*advertisement*" in accordance with 18 U.S.C. Section 1734 solely to indicate this fact.

direct tonic model of ocular counterroll. Like Glasauer et al. (2001), we started with a previously published model of the 3-D saccade generator (Crawford and Guitton 1997), and then modified it to produce counterroll. The mathematical details of our modifications are described in the DATA SUPPLEMENTS section, and schematic versions of our two models are provided in Fig. 1, *A* and *F*. In both models, the saccadic pulse generator projects to the motoneurons both directly and by the neural integrator. Recall that in the direct tonic model (Fig. 1*A*), the otolith organs project directly to the motoneurons. In contrast, with our version of the integrated pulse model, the otolith signals project to the saccadic pulse generator (Fig. 1*F*).

The remainder of Fig. 1 illustrates simulations generated by these models. As we shall see, it is difficult to distinguish between these models on the basis of simulated behavior, until the torsional neural integrator malfunctions. Here we define torsion as roll of the eye about a head-fixed axis parallel to gaze direction at the primary position (Tweed et al. 1990). Each simulation plots this torsional component of eye position versus the horizontal component (n) (represented as quaternions; Westheimer 1957) during a series of 1-s postsaccadic fixation periods. (This type of plot is standard in 3-D eye movement studies that use quaternion or rotation vectors.) The saccades themselves are not shown. Figure 1, *B* and *G* shows the eye positions generated with the head upright; these are identical in the two models because both use a Listing's law operator (Tweed and Vilis 1990b) to set torsional eye positions at zero for all combinations of horizontal (and vertical) eye position. This results in a 2-D range of eye positions called *Listing's plane* (Ferman et al. 1987; Straumann et al. 1991; Tweed and Vilis 1990a).

Figure 1, *C* and *H* show the eye positions when the head is rotated 90° CCW: both models now counterroll the eyes 10° CW. In Fig. 1*C* (*direct tonic* model) the eye counterrolls because the otoliths are directly activating the appropriate eye muscles. In Fig. 1*H* (*integrated pulse* model) the eye counterrolls because the tonic otolith signal modifies the Listing's law operator to specify a torsionally shifted plane of eye positions (Glasauer et al. 2001). This results in a pulsatile saccade command with a torsional component that is equal and opposite to any initial deviation from this plane. This pulse is then integrated to produce the eye position that maintains counterroll. Either way, this manifests itself as a torsional shift in Listing's plane (Fig. 1*H*)—as seen in real data (Crawford and Vilis 1991; Haslwanter et al. 1992)—but this still looks the same for both models.

The remaining panels simulate integrator failure. Experimentally, the torsional and vertical integrators can be inacti-

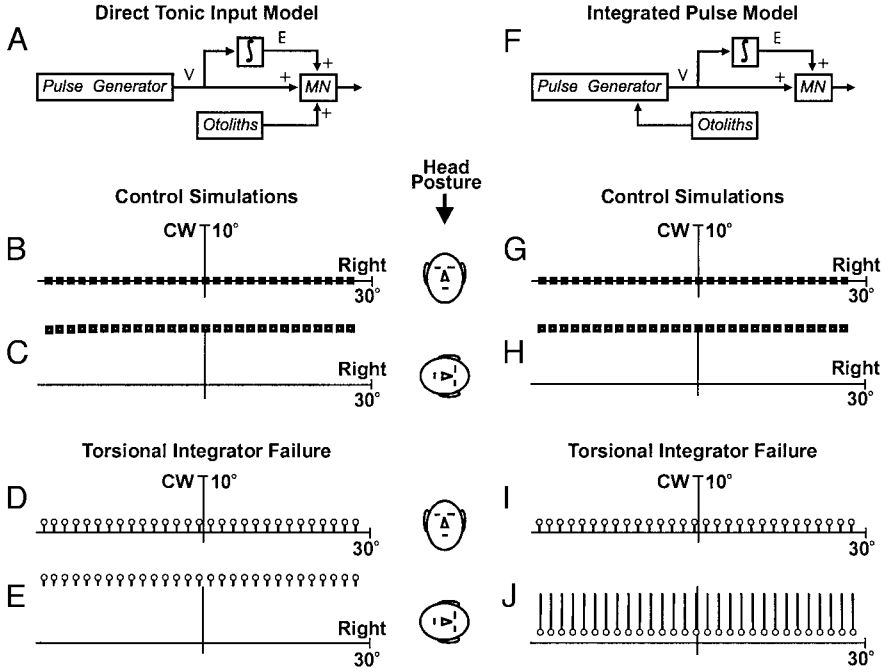

FIG. 1. Simulated test between two models of ocular counterroll (*left column* vs. *right column*). *A*: schematic representation of direct tonic input model, used for simulations. For this model, a scaled version of torsional head-tilt signal was simply added to appropriate motoneuron signal. *B–E*: only simulated fixations between saccades are shown. These saccades started with eye 28° leftward, and brought eye rightward in 2° steps. Torsion is defined as rotation about head-fixed axis parallel to gaze at primary position, and is plotted as function of horizontal eye-in-head position. Head posture upright or tilted 90° as indicated. *B*: control fixation points (■) in Listing's plane. *C*: fixation points during ocular counterroll, simulated by adding tonic torsional signal (from otoliths) to signals summating at motoneurons. *D*: simulated unilateral torsional integrator damage, where eye drifts (■) torsionally (but not horizontally) toward final resting positions (○) that form *equilibrium range* (Crawford and Vilis 1993). Saccades (not shown) bring eye back to Listing's plane. Torsional integrator was completely inactivated and eye was given period of 5 s to drift at mechanical time constant of plant between saccades, so technically drift reaches 99.9% of way to equilibrium position. *E*: identical integrator failure combined with tonic motoneuron inputs shown in *C*. Entire pattern of drift and equilibrium range shift. *F*: indirect integrated pulse model [see supplementary data and Glasauer et al. (2001) for details], used to generate simulations *G–J*, which correspond to same conditions described for *B–E*, but counterrolled fixation points (*H*) were simulated by phasic commands directing saccades to torsionally shifted range of desired eye positions. Combined with integrator deficit (*J*) these saccades still drove eye to shifted range, but eye then drifted back toward same unshifted equilibrium range as shown in *I*. This differs from corresponding prediction of other model (*E*).

vated by injecting muscimol, a GABA agonist, into the interstitial nucleus of Cajal (INC) (Crawford et al. 1991; Helmchen et al. 1998). Even unilateral injection into the INC has this effect (Crawford et al. 1991), presumably because the two sides of the integrator are interdependent (Anastasio and Robinson 1991; Galiana and Outerbridge 1984). During such deficits, ocular torsion drifts toward an "equilibrium value," usually a slightly CW value after left-sided injection and a CCW value after right-sided injection (Crawford 1994; Crawford and Vilis 1993). This is thought to be attributed to a loss of integrating ability and a torsional imbalance in the remaining vestibular drive (Cannon and Robinson 1985; Crawford 1994). In Fig. 1, this was simulated by inputting a constant torsional offset to the integrator and reducing its time constant below that of the eye muscles. This resulted in CW drift toward a set of torsionally shifted equilibrium points (open circles) in Fig. 1, *D* and *I*. Because horizontal position holding remained intact, this produced a *line* of equilibrium positions, which we call the *equilibrium range* (Crawford and Vilis 1993).

When the head rolls 90° CCW (Fig. 1, *E* and *J*), the two models now yield very different predictions. In Fig. 1*E*, the equilibrium range has shifted 10° farther CW than in Fig. 1*D* as a consequence of counterroll. In Fig. 1*J*, the equilibrium range is unmoved because counterroll is unable to act through the malfunctioning integrator. There are other differences between the predictions—for instance, the torsional drift is CW in Fig. 1*E* and CCW in Fig. 1*J*—but these are lesser matters that depend on the properties of the saccadic pulse generator in the model. The crucial prediction—the one that holds regardless of the properties pulse generator itself—is this: if counterroll is caused by direct tonic input to motoneurons, then rolling the head during integrator failure should shift the eye's torsional equilibrium range, whereas if counterroll is implemented by an integrated pulse, then rolling the head during integrator failure should have no effect on the equilibrium range (Crawford and Vilis 1999; Glasauer et al. 2001). Thus the equilibrium range (open circles) shifted torsionally between Fig. 1, *D* and *E* (*direct tonic* model), but not between Fig. 1, *I* and *J* (*integrated pulse* model). Our experiment was designed to test between these two predicted results.

METHODS

General experimental procedures

Experiments were performed on 2 alert, behaving monkeys (M1 and M2, *Macaca fascicularis*). The details of our general procedures were reported elsewhere (Crawford 1994; Crawford and Vilis 1993; Crawford et al. 1991); here we provide an overview. Experiments were done in accordance with the guidelines of the Canadian Council on Animal Care and were approved by the University of Western Ontario Animal Care Committee. Each monkey underwent surgery under aseptic conditions and pentobarbital anesthesia. A skullcap of dental acrylic was fastened to the animal's head, and 2 enameled copper search coils 5 mm across were implanted in one eye (in animal M2) or both (in M1). Wire leads from the coils ran temporally beneath the conjunctiva and then subcutaneously to sockets on the cap.

Eye movements were recorded at 100 Hz using double search coils in three magnetic fields (Robinson 1963; Tweed 1990) with the monkey's head immobilized near the center of the fields. Coil signals were converted into quaternion vectors, whose 3 components express the torsional, vertical, and horizontal components of eye position (Tweed et al. 1990). First computed in "field coordinates," where the *x*-, *y*-, and *z*-axes are aligned with the magnetic fields, these vectors were then converted to more physiologically meaningful "Listing coordinates" in which the zero vector represents primary position and the positive *x*-axis coincides with the primary gaze direction (Tweed et al. 1990). One such Listing coordinate system was used to express all the data collected in any given experiment.

A recording chamber was mounted stereotaxically over the INC (Shantha et al. 1968). For cell recording, a monopolar tungsten electrode (Frederick Haer, 4 MΩ) was manually advanced, together with a guide tube, to within 5 mm of the selected oculomotor region and was then extruded by as much as 10 mm beyond the tube by a hydraulic microdrive. The INC was identified by comparing neuronal discharge with eye movements and positions, and then microstimulating at 20 μA for 200-ms trains (Crawford et al. 1991). The INC was characterized functionally as a region containing a mixture of vertical eye position and velocity signals (Dalezios et al. 1998; King et al. 1981), which, when stimulated, produced conjugate torsional eye movements that hold their final position until corrected by a saccade (Crawford et al. 1991).

Then the electrode was withdrawn from its guide tube and a 30-gauge cannula was lowered through the tube, usually to the top of the region of oculomotor activity. A Hamilton syringe was used to deliver 0.3 μl of a 0.05% muscimol solution, which inhibits local cell bodies without affecting fibers of passage. [Injection controls and more detailed criteria distinguishing the INC from surrounding structures like the riMLF and 3rd cranial-nerve nucleus were published in Crawford and Vilis (1992, 1993) and Crawford et al. (1991).] Eye movement recordings commenced immediately and continued for 30 min or more. Afterward the animal recovered for 48 h (no muscimol effects persisted that long) before experiments were repeated at an adjacent brain site 1-mm lateral–medial or rostral–caudal.

After all experiments were complete, the animals were deeply anesthetized with pentobarbital. Electrolytic lesions (1.5 mA anodal current for 15 s) were made at a reference microdrive coordinate and immediately afterward animals were given a lethal dose of anesthetic and perfused with formalin. The brains were removed, sliced into 100-μm sections, and stained with thionine. The resulting slides were compared with a stereotaxic atlas of the monkey brain (Shantha et al. 1968) to confirm histologically our functional identification of the INC.

Experimental protocol

Our goal was to compare normal counterroll with that seen during torsional integrator failure. To define each animal's normal range of torsion, we recorded its eye movements as it made pseudo-random saccades for 100 s between visual targets presented throughout the oculomotor range. We then tilted the animal's whole body in two different positions—90° left ear down and 90° right ear down—and again recorded its eye positions as it looked at targets throughout the oculomotor range. This procedure was repeated on 5 days with each animal to establish control levels of counterroll.

We then repeated these procedures during integrator failure. Muscimol was injected near the lateral upper border of the INC. Data were collected within 1 h of injection, before the drug could spread to the deeper, more medial motoneurons of cranial-nerve nucleus III. After injections, eye movements were monitored with the monkey upright until the torsional integrator began to fail (i.e., until the eyes began to drift torsionally). As described previously (Crawford 1994; Crawford and Vilis 1993; Crawford et al. 1991), the temporal trajectories of this drift were indicative of neural integrator failure.

The animal was then rolled 90° CW, CCW, or both (when the progress of the muscimol effect allowed enough time), and its eye movements were recorded to see whether its torsional equilibrium position was affected by body position. Afterward the animal was returned to the upright posture and a final measurement was taken to check the stability of the equilibrium position across time. A total of

11 such muscimol injection experiments were performed in animal M1 and 7 in M2.

RESULTS

Figure 2 shows eye-position data analogous to the simulations in Fig. 1, plotted using similar conventions in head-fixed Listing coordinates. Again, spatial plots are provided to simultaneously compare a large number of movements and view the whole equilibrium range. Torsional components of eye position are plotted versus horizontal components in the *left column*, and versus vertical in the *right column*. Cartoon heads show the position the monkey was in while the data in each row were recorded. Figure 2, *A* and *B* shows monkey M1's eye positions during postsaccadic fixations with the head upright, as simulated in Fig. 1*B*. When the animal is tilted 90° CCW, in Fig. 2, *C* and *D*, its whole range of eye positions is counterrolled about 10° CW, as in Fig. 1, *C* and *H*.

The remainder of Fig. 2 shows data from the same animal after an injection of muscimol into the right INC. Linear tracks show the eye's drift between saccades, with circles marking the final eye position before the next saccade. The range of final eye positions is somewhat larger than the equilibrium range (quantified below) because the intersaccadic intervals were often too brief to allow the drift to settle. Figure 2, *E* and *F* shows torsional and vertical postsaccadic drift with the head upright, roughly analogous to the drift simulated in Fig. 1, *D* and *I*. The details of this result have been thoroughly reported elsewhere (Crawford 1994; Crawford and Vilis 1993; Crawford et al. 1991).

The pertinent question here is, what happens to the drift when the head is tilted 90° CCW? According to the *direct tonic* model (Fig. 1*E*), we should see the same pattern as in Fig. 2, *E* and *F*, but shifted as far as the counterroll in Fig. 2, *C* and *D*, about 10° CW. This was not observed. Instead, Fig. 2, *G* and *H* conform to the pattern predicted by the integrated pulse model (Fig. 1*J*): the eyes drift CCW to a range that is hardly shifted from its position when the head was upright. In other words, the counterroll exhibited by this monkey in Fig. 2, *C* and *D* is virtually eliminated during integrator failure—at least for the drift endpoints. Clearly, this lack of counterroll was not the result of some paralysis of CW-pulling eye muscles because saccades still attained CW positions (i.e., the drifts began far CW). Finally, when the head is returned to the upright position, in Fig. 2, *I* and *J*, the drift returns to the pattern observed in the control (Fig. 2, *E* and *F*).

Qualitatively, then, the data closely match the prediction of the integrated pulse model. Again, some details of the nystagmus pattern were complicated by extraneous factors such as a progressive imbalance in the CW/CCW burst generator (Crawford and Vilis 1993), but a clean test of the two models is the shift in the torsional equilibrium range. For the purpose of this experiment, we defined this range to be those positions sampled when eye velocity was $\leq 0.25°/s$.

Figure 3, *A–C* shows a typical equilibrium range during integrator failure; before, during, and after CCW head tilt, respectively. Only the equilibrium points (velocity $\leq 0.25°/s$) are shown here; the drift segments are not shown because they tend to obscure this range. Curved lines show the intersection of the second-order surface fit with the vertical position = zero plane, used here to indicate the "equilibrium line" discussed above. In this experiment, muscimol was injected into the right INC, shifting the equilibrium range CCW. The range was unmoved when the head tilted 90° CCW, that is, counterroll was absent in this range (Fig. 3*B*). This is clearly not because

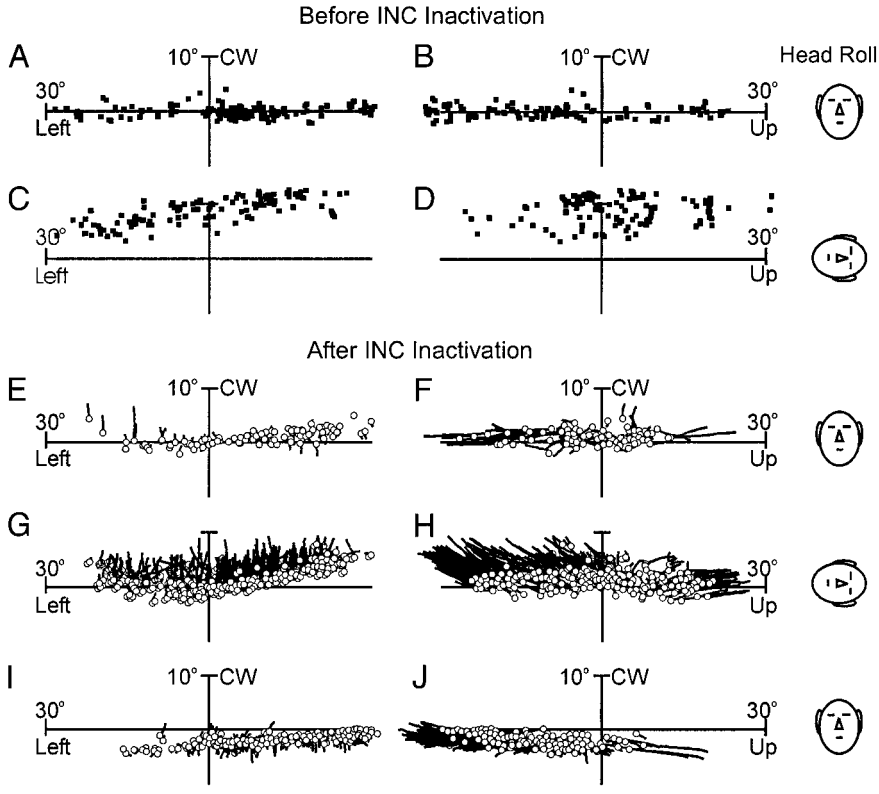

FIG. 2. Actual result of test shown in Fig. 1, using similar plotting conventions. Ocular torsion in animal M1 is plotted in Listing's plane coordinates as function of horizontal position (*left column*) and vertical position (*right column*). *A* and *B*: control fixations (eye velocity $<1°/s$) between saccades with head upright. *C* and *D*: clockwise (CW) ocular counterroll of eye position range during 90° counterclockwise (CCW) head posture. (○): endpoint of each drift segment, which was generally close to but not necessarily equal to equilibrium resting range. *E* and *F*: ocular drift and drift endpoints between saccades, 34 min after injection of muscimol into right interstitial nucleus of Cajal. *G* and *H*: changes in drift pattern during 90° CCW head tilt. *I* and *J*: drift after returning head to upright posture.

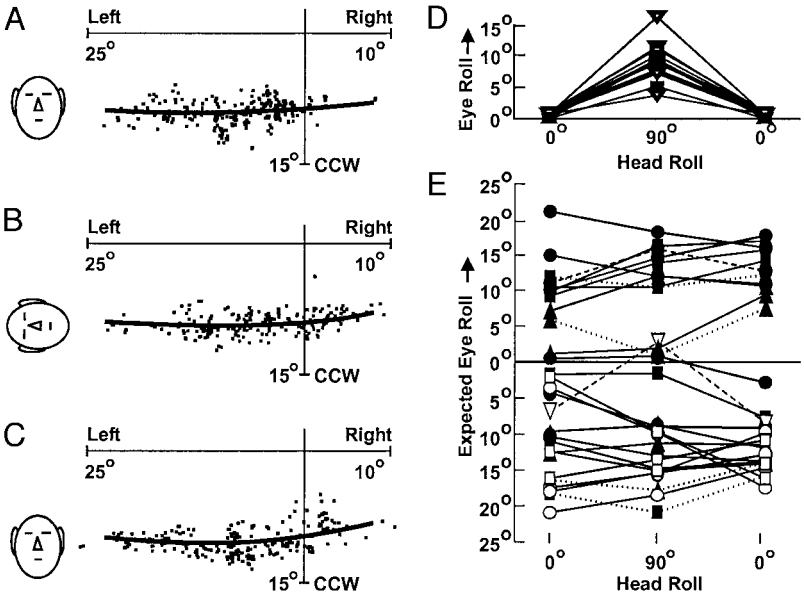

FIG. 3. Counterclockwise (CCW) shifted equilibrium range of resting eye positions (eye velocity <0.25°/s) after injection of muscimol in right interstitial nucleus of Cajal in animal M2; before (*A*), during (*B*), and after (*C*) 90° CCW head roll. These measureiments were initiated 10, 20, and 28 min after muscimol injection, respectively. Curved lines show intersection of the second-order surface fit with vertical position = zero plane, used here to indicate "equilibrium line" discussed above. Equilibrium range failed to shift clockwise during head roll. *D* and *E*: quantitative test between models looking at amount of shift in equilibrium range. *D*: torsional shift of eye range (direction normalized so that + is normal direction of counterroll) in intact animal with head upright or tilted 90°. *E*: normalized equilibrium range shifts after injection of muscimol into interstitial nucleus of Cajal, before, during, and after a 90° torsional roll in head posture. Again, equilibrium range failed to show systematic counterroll. Two experiments showed a positive peak consistent with preserved counterroll (dashed line) but 4 showed opposite negative peak (dotted line), so these are probably unrelated drifts in equilibrium range across time. Circles: M1, left eye; squares: M1, right eye; triangles: M2; filled symbols: head CCW; unfilled symbols: head CW.

of any torsional saturation, given that in this case counterroll (had it occurred) would have rolled the eye *toward* zero torsion.

To quantify the shift in these ranges we fitted second-order surfaces (Glenn and Vilis 1992) to the equilibrium positions. The overall torsional shifts in the null range relative to Listing's plane were quantified by the first parameter of the second-order surface fit (i.e., the distance of the surface from Listing's plane at zero horizontal and zero vertical). Table 1 in the DATA SUPPLEMENTS reports these values for all 18 of our muscimol experiments, before, during, and after head tilts (see the Supplemental Material, available at the *Journal of Neurophysiology* website).[1] However, it is tedious to compare these values to the predicted counterroll of the direct tonic model, which is sometimes negative and sometimes positive. Therefore for simpler visual comparison with the models' predictions, we plot, in Fig. 3, *D* and *E*, *normalized* shift data, in which positive torsion is defined as torsion in the direction opposite to head tilt (i.e., in the expected direction of ocular counterroll).

Figure 3*D* shows control levels of counterroll: normalized torsional offsets before muscimol injection, before and during 90° head tilt. The before values were zero by definition. The "after value" simply repeats this measurement for the sake of visual consistency with Fig. 3*B* (the torsional offset of Listing's plane does not vary significantly over short time spans). However, as shown by the central peaks, the eye consistently counterrolled during head tilt. Across experiments, counterroll was 8.6 ± 0.5° (mean and SE in degrees for monkey M1, left eye), 8.5 ± 0.9° (M1, right eye), 8.5 ± 2.2° (monkey M2), and 8.5 ± 0.7° (all data, averaged together). This counterroll was significantly larger than zero in every measurement ($P \leq 0.017$).

Figure 3*E* shows the absence of counterroll in the torsional equilibrium range after muscimol injection. Most experiments showed a bias in the equilibrium range, which depended on the injection site but was largely uninfluenced by head roll. The normal counterroll pattern from Fig. 3*A*, with its central peak rising some 8.5°, was absent in almost all experiments here. Positive peaks consistent with counterroll were observed in only two cases (dashed line), whereas opposite, negative peaks were observed in four cases (dotted line), suggesting that all of these peaks may have been attributed to random fluctuations in the equilibrium range as the integrator deficit progressed. On average, counterroll amounted to only 0.3 ± 0.6° (monkey M1, left eye), −0.1 ± 0.9° (M1, right eye), 0.7 ± 2.0° (monkey M2), and 0.3 ± 0.6° (averaged across all data). It was never close to statistical significance in any measurement, even when all the data were treated as one population ($P = 0.67$).

DISCUSSION

We have shown that during neural integrator failure, the torsional equilibrium range fails to counterroll during head tilt. This finding contradicts the view that counterroll is driven by direct tonic inputs from the otolith organs to the motoneurons, but rather implies that counterroll is implemented through the neural integrator (Crawford and Vilis 1991; Glasauer et al. 2001). We do not claim this to be the only issue associated with ocular counterroll—for example, the model proposed by Glasauer et al. (1998) explains several aspects of patient data not touched on here—but this does provide a central constraint for future theoretical and physiological investigations.

Although the current study is the first to provide a detailed kinematic analysis of ocular counterroll during torsionally integrator failure, we acknowledge that a previous study briefly reported a similar experiment (Helmchen et al. 1998). Surprisingly, these authors drew conclusions that at first glance seem directly opposite to that drawn here; that is, they concluded that counterroll is preserved during INC inactivation. However, that report did not make the distinction (shown here to be crucial) between the equilibrium range and the entire position range. Apparently they analyzed the latter, which could yield a different result (see Fig. 2). There are also methodological differences: we used much larger head tilts to optimize our test. Finally, the Helmchen study tested only a handful of muscimol/INC injections during head roll—perhaps missing the crit-

[1]The Supplementary Material for this article (a table) is available online at http://jn.physiology.org/cgi/content/full/00231.2003/DC1

ical site—and did not provide any graphic or quantitative data to substantiate their report. Therefore we are not convinced that this previous study negates the findings documented here.

Another previous study seems to contradict the particular model simulated here, that is, where saccadic burst neurons provide this torsional pulse. Suzuki et al. (1995) showed that counterroll persisted after lesions of the saccade-related burst neurons in the riMLF. If it were not for this result, riMLF burst neurons would have seemed to be the ideal source of the torsional pulse in our model. However, although the riMLF is probably required to generate the pulse for torsional quick phase movements (Crawford and Vilis 1992; Henn et al. 1989), the pulsatile signals required for counterroll probably originate from more vestibular-related structures. Therefore Suzuki et al. (1995) does not contradict the integrated pulse model; it just contradicts the idea that this counterrolling pulse originates from the riMLF.

A third potential problem for our model arises from reports suggesting that the torsional integrator is too leaky to hold a sustained, uninterrupted counterroll (Glasauer et al. 2001; Seidman et al. 1995). For example, there is currently no evidence that the time constant of the integrator response to a torsional VOR step is >7 s (S. H. Seidman, personal communication). However, the integrator may be more complex than a first-order, linear low-pass filter and may show different time constants for different inputs.

A second solution to this problem would be to provide an additional tonic torsional input from the otoliths to the integrator, with just enough gain to overcome the slight normal tendency of the torsional integrator to leak backward (Glasauer et al. 2001). (Note, however, that this path would not have enough gain to overcome the severe integrator leak that we induced in the current study.) Such a tonic path might account for observations of counterroll in the absence of saccades (Clarke et al. 1999), and—in combination with a leaky integrator—it would tend to produce frequency-dependent torsional effects perhaps consistent with the reports of Hess and Angelaki (1997b). It would also produce a nonlinear gain (i.e., with reduced counterroll gain for larger head tilts), which appears to be correct. However, if such a path exists, it does not appear to be anatomically direct (Sasaki et al. 1991; Uchino et al. 1996), and one would still require a concomitant adjustment to the torsional set point of the saccade generator, for reasons that we will discuss in the next section.

Finally, an integrator time constant of several seconds is still a long time compared with the intersaccadic interval—if, as we argue in the next section, some part of the saccadic pulse generator (other than the riMLF) contributes to counterroll. Very little torsional drift would occur in the typical 200–300 ms between saccades. Moreover, the INC integrator appears to have a parallel architecture with different time constants in the parallel modules (Cannon and Robinson 1985; Crawford and Vilis 1993; Helmchen et al. 1998), so repeated phasic inputs from the saccade generator would tend to charge such an integrator array up to the desired set point with less and less postsaccadic drift (Crawford and Vilis 1993). Such a parallel architecture would also explain why it is that following the dynamic vestibulo-ocular reflex (VOR) response to a torsional step in head position (if saccades are suppressed), the eye drifts partway back to the ocular torsion observed during sustained counterroll and holds this intermediate position (Kori et al. 2001; see Fig. 1). It would be valuable to test whether subsequent saccades would then bring the eye back toward a final counterroll set point, with progressive reductions in the amount of postsaccadic torsional drift.

Counterroll and saccades

What is the source of the counterroll command that feeds into the integrator? There may be multiple sources, although there are theoretical reasons to believe that these signals are associated with the rapid eye movement generator (where this term incorporates all of the saccadic and vestibular signals that would normally be active during a head-free gaze shift). The rapid eye movement system should be able to drive the eyes to counterrolled positions. Otherwise, whenever you shifted your gaze while lying on your side, you would have torsional postsaccadic drift. Anecdotal evidence that rapid eye movements implement counterroll can be seen in Fig. 2, *G* and *H*, where the drifts begin from eye positions that are shifted nearly 10° CW (i.e., the rapid eye movements deliver the eyes to counterrolled positions). Unfortunately, this result depends on the existence of an intact burst generator, whereas most of our other INC injections resulted in a torsional imbalance in the saccade generator, besides integrator failure (Crawford and Vilis 1993).

However, there is another more fundamental reason to suggest that counterroll circuits are involved in rapid eye movement generation (Crawford and Vilis 1991; Vilis 1993). If they were not, one would expect this system to try to correct the counterroll produced by the neural integrator (no matter what the original source of this signal), as it does for similar torsion produced by the dynamic VOR, electrical stimulation of the brain stem, or the optokinetic reflex (Lee et al. 2000). Instead, the final torsional quick phase at the end of a dynamic head tilt brings the eye to a counterrolled position (otherwise there would be no counterroll!) as do the torsional "saccades" in Fig. 2, *G* and *H*. In other words, if the saccade generator "knows" about counterroll, as it almost certainly does (Klier and Crawford 1998), then it is hard to avoid the conclusion that it "wants" and maintains this level of counterroll. Similar arguments could hold for the smooth pursuit system, which obeys Listing's law with the head upright (Haslwanter et al. 1991; Tweed et al. 1992) and might share similar "Listing's operator" circuitry, but has not been so thoroughly tested at other head postures.

The solution to these problems is to allow the internal selection of Listing's plane to depend on inputs from the vestibular system (Crawford et al. 1991; Glasauer et al. 2001). In the DATA SUPPLEMENTS we show how this idea can be modeled using an adjustable Donders operator, a neural structure that selects target eye positions for saccades and selects different torsional orientations depending on head tilt (and perhaps depending on other factors as well). Donders's law is the more general form of Listing's law, where the latter may be modified under different circumstances to produce different 2-D ranges of eye position, to optimize different functional constraints. We know, for instance, that the saccadic system chooses different torsional eye positions when the eyes are converged to view near targets (Mok et al. 1992; Van Rijn and Van Den Berg 1993).

These arguments suggest that the pathway for counterroll

involves elements of the rapid eye movement generator—in the broad sense. These pathways would presumably be incorporated within the polysynaptic otolith–motoneuron connections reported by Uchino et al. (1996). In our view, likely candidates include the NRTP/cerebellum (Van Opstal et al. 1996), vestibular-related burst-driver neurons in the INC and elsewhere (Helmchen et al. 1998; Kaneko and Fukushima 1998; Kitama et al. 1995), and perhaps the midbrain MRF region (Waitzman et al. 1996). However, this is currently just speculation; as pointed out in the INTRODUCTION, there are many possible ways to input a counterrolling pulse to the neural integrator.

Function of ocular counterroll

Finally, we further speculate that the rapid eye movement system may explain why humans and other primates have counterroll at all. Human counterroll is far too weak to fulfill the role it presumably played in our distant ancestors (Baarsma and Collewijn 1975; Dickman and Angelaki 1999), that is, keeping the horizontal retinal meridian aligned with the horizon. Further, counterroll is positively disruptive for binocular vision (Misslisch et al. 2001). So why has an obsolete, harmful reflex survived for millennia in the primate brain? Perhaps it has survived because it has found a new function. Certainly it is well suited to improve the efficiency of eye-head gaze shifts.

Whenever we make a gaze shift involving torsional, say CW, head motion, our eyes rotate CW in our heads so as to arrive more quickly at their target orientation in space (Tweed et al. 1998). Now when your head is tilted left ear down, or CCW, chances are your next eye-head gaze shift will be CW rather than further CCW. In other words, the rapid eye movement system has statistical grounds to expect a CW gaze shift. It is thus advantageous to poise the eyes in a CW, counterrolled position, to give them a head start in their upcoming saccade. Our current view, then, is that the rapid eye movement generator has adopted the ocular counterroll reflex as a way of positioning the eye to prepare for the torsional components of head-free gaze shifts.

DISCLOSURES

This work was funded by Canadian Institutes for Health Research Grant MOP13357 and Canadian Medical Research Council Grant MT9335. J. D. Crawford is supported by a Canada Research Chair.

REFERENCES

Anastasio TJ and Robinson DA. Failure of the oculomotor neural integrator from a discrete midline lesion between the abducens nuclei in the monkey. *Neurosci Lett* 127: 82–86, 1991.

Angelaki DE, McHenry MQ, Dickman JD, Newlands SD, and Hess BJ. Computation of inertial motion: neural strategies to resolve ambiguous otolith information. *J Neurosci* 19: 316–327, 1999.

Baarsma E and Collewijn H. Eye movements due to linear accelerations in the rabbit. *J Physiol* 245: 227–247, 1975.

Bockisch CJ and Haslwanter T. Three-dimensional eye position during static roll and pitch in humans. *Vision Res* 41: 2127–2137, 2001.

Brandt T and Dieterich M. Vestibular syndromes in the roll plane: topographic diagnosis from brainstem to cortex. *Ann Neurol* 36: 337–347, 1994.

Cannon SC and Robinson DA. An improved neural-network model for the neural integrator of the oculomotor system: more realistic neuron behavior. *Biol Cybern* 53: 93–108, 1985.

Clarke AH, Engelhorn A, Hamann CH, and Schönfeld U. Measuring the otolith-ocular response by means of unilateral radial acceleration. *Ann NY Acad Sci* 871: 387–391, 1999.

Crawford JD. The oculomotor neural integrator uses a behavior-related coordinate system. *J Neurosci 14*: 6911–6923, 1994.

Crawford JD, Ceylan MZ, Klier EM, and Guitton D. Three-dimensional eye-head coordination during gaze saccades in the primate. *J Neurophysiol* 81: 1760–1782, 1999.

Crawford JD and Guitton D. Visuomotor transformations required for accurate and kinematically correct saccades. *J Neurophysiol* 78: 1447–1467, 1997.

Crawford JD and Vilis T. Axes of eye rotation and Listing's law during rotations of the head. *J Neurophysiol* 65: 407–423, 1991.

Crawford JD and Vilis T. Modularity and parallel processing in the oculomotor integrator. *Exp Brain Res* 96: 443–456, 1993.

Crawford JD and Vilis T. Role of the 3-D neural integrator in control of ocular counterroll. *Soc Neurosci Abstr* 25: 6, 1999.

Collewijn H, Van Der Steen J, Ferman L, and Jansen TC. Human ocular counterroll: assessment of static and dynamic properties from electromagnetic scleral coil recordings. *Exp Brain Res* 59: 185–196, 1985.

Dalezios Y, Scudder CA, Highstein SM, and Moschovakis AK. Anatomy and physiology of the primate interstitial nucleus of Cajal. II. Discharge pattern of single efferent fibers. *J Neurophysiol* 80: 3100–3111, 1998.

Dickman JD and Agnelaki DE. Three-dimensional organization of vestibular related eye movements to off-vertical axis rotation and linear translation in pigeons. *Exp Brain Res* 129: 391–400, 1999.

Ferman L, Collewijn H, and Van den Berg AV. A direct test of Listing's law. I. Human ocular torsion measured in static tertiary positions. *Vision Res* 27: 929–938, 1987.

Fukushima K and Kaneko CR. Vestibular integrators in the oculomotor system. *Neurosci Res* 22: 249–258, 1995.

Fukushima K, Ohashi T, Fukushima J, and Kase M. Ocular torsion produced by unilateral chemical inactivation of the interstitial nucleus of Cajal in chronically labyrinthectomized cats. *Neurosci Res* 13: 301–305, 1992.

Furman JM and Schor RH. Oirentation of Listing's plane during static tilt in young and odler human subjects. *Vision Res* 43: 67–76, 2003.

Galiana HL, and Outerbridge JS. A bilateral model for central neural pathways in vestibuloocular reflex. *J Neurophysiol* 51:210–241, 1984.

Glasauer S, Dieterich M, and Brandt T. Three-dimensional modeling of static vestibulo-ocular brain stem syndromes. *Neuroreport* 9: 3841–3845, 1998.

Glasauer S, Dieterich M, and Brandt T. Central positional nystagmus simulated by a mathematical ocular motor model of otolith-dependent modification of Listing's plane. *J Neurophysiol* 86: 1546–1554, 2001.

Glenn B and Vilis T. Violations of Listing's law after large eye and head gaze shifts. *J Neurophysiol* 68: 309–317, 1992.

Haslwanter Th. Mathematics of three-dimensional eye rotations. *Vision Res* 35: 1727–1739, 1995.

Haslwanter T, Straumann D, Hepp K, Hess BJ, and Henn V. Smooth pursuit eye movements obey Listing's law in the monkey. *Exp Brain Res* 87: 470–472, 1991.

Haslwanter Th, Straumann D, Hess BJM, and Henn V. Does counterrolling violate Listing's law? *Ann NY Acad Sci* 656: 931–932, 1992.

Helmchen C, Rambold H, and Büttner U. Saccade-related burst neurons with torsional and vertical on-directions in the interstitial nucleus of Cajal in the alert monkey. *Exp Brain Res* 112: 63–78, 1996.

Helmchen C, Rambold H, Fuhry L, and Buttner U. Deficits in vertical and torsional eye movements after uni- and bilateral muscimol inactivation of the interstitial nucleus of Cajal of the alert monkey. *Exp Brain Res* 119: 436–452, 1998.

Hess BJM and Angelaki DE. Kinematic principles of primate rotational vestibulo-ocular reflex. I. Spatial organization of fast phase velocity axes. *J Neurophysiol* 78: 2193–2202, 1997a.

Hess BJM and Angelaki DE. Kinematic principles of primate rotational vestibulo-ocular reflex. II. Gravity-dependent modulation of primary eye position. *J Neurophysiol* 78: 2203–2216, 1997b.

Hess BJM and Angelaki DE. Dynamic control of primary eye position as a function of head orientation relative to gravity. In: *Three-Dimensional Kinematics of Eye, Head and Limb Movements*, edited by Fetter M, Haslwanter T, Misslisch H, and Tweed D. Amsterdam: Harwood, 1997c, p. 177–185.

Hess BJM and Angelaki DE. Oculomotor control of primary eye position discriminates between translation and tilt. *J Neurophysiol* 81: 394–398, 1999.

Kaneko CRS and Fukushima K. Discharge characteristics of vestibular saccade neurons in alert monkeys. *J Neurophysiol* 79: 835–847, 1998.

King WM, Fuchs AF, and Magnin M. Vertical eye movement-related responses of neurons in midbrain near interstitial nucleus of Cajal. *J Neurophysiol* 46: 549–562, 1981.

Kitama T, Ohki Y, Shimazu H, Tanaka M, and Yoshida K. Site of interaction between saccade signals and vestibular signals induced by head rotation in the alert cat: functional properties and afferent organization of burster-driving neurons. *J Neurophysiol* 74: 273–287, 1995.

Klier EM and Crawford JD. The human oculomotor system accounts for 3-D eye orientation in the visual-motor transformation for saccades. *J Neurophysiol* 80: 2274–2294, 1998.

Kori AA, Schmid-Priscoveanu A, and Straumann D. Vertical divergence and counterroll eye movements evoked by whole-body steps about the roll axis of the head in humans. *J Neurophysiol* 85: 671–678, 2001.

Lee C, Zee DS, and Straumann D. Saccades from torsional offset positions back to Listing's plane. *J Neurophysiol* 83: 3241–3253, 2000.

Misslisch H, Tweed D, and Hess BJM. Stereopsis outweighs gravity in the control of the eyes. *J Neurosci* 21: RC126, 2001.

Ott D. Vestibular– neck interaction of human ocular counterroll. *Behav Brain Res* 48: 87–90, 1992.

Paige GD and Tomko DL. Eye movement responses to linear head motion in squirrel monkey. I. Basic characteristics. *J Neurophysiol* 65: 1170–1182, 1991.

Robinson DA. Oculomotor control signals. In: *Basic Mechanisms of Ocular Motility and Their Clinical Implications*, edited by Bach-y-Rita P and Lennerstrand G. (Wenner-Gren Cent. Int. Symp. Ser.) Oxford, UK: Pergamon, 1975, p. 337–374.

Sasaki M, Hiranuma K, Isu N, and Uchino Y. Is there a three neuron arc in the cat utriculo-trochlear pathway? *Exp Brain Res* 86: 421–425, 1991.

Schor RH, Miller AD, and Tomko DL. Responses to head tilt in cat central vestibular neurons. I. Direction of maximum sensitivity. *J Neurophysiol* 51: 136–146, 1984.

Seidman SH, Leigh RJ, Tomsak L, Grant P, and Dell'Osso LF. Dynamic properties of the human vestibulo-ocular reflex during head rotations in roll. *Vision Res* 35: 679–689, 1995.

Straumann D, Haslwanter Th, Hepp-Reymond M-C, and Hepp K. Listing's law for the eye, head and arm movements and their synergistic control. *Exp Brain Res* 86: 209–215, 1991.

Suzuki Y, Büttner-Ennever JA, Straumann D, Hepp K, Hess BJM, and Henn V. Deficits in torsional and vertical rapid eye movements and shift of Listing's plane after uni- and bilateral lesions of the rostral interstitial nucleus of the medial longitudinal fasciculus. *Exp Brain Res* 106: 215–232, 1995.

Telford L, Seidman SH, and Paige GD. Dynamics of squirrel monkey linear vestibulo-ocular reflex and interactions with fixation distance. *J Neurophysiol* 78: 1775–1790, 1997.

Theeuwen M, Miller LE, and Gielen CCAM Is the orientation of head and arm coupled during pointing movements? *J Motor Behav* 25: 242–250, 1993.

Tomko DL, Peterka RJ, and Schor RH. Responses to head tilt in cat eighth nerve afferents. *Exp Brain Res* 41: 216–221, 1981.

Tweed D, Fetter M, Andreadaki S, Koeneg E, and Dichgans J. Three-dimensional properties of human pursuit eye movements. *Vision Res* 32: 1225–1238, 1992.

Tweed D, Haslwanter T, and Fetter M. Optimizing gaze control in three dimensions. *Science* 281: 1363–1366, 1998.

Tweed D and Vilis T. Implications of rotational kinematics for the oculomotor system in three dimensions. *J Neurophysiol* 58: 832–849, 1987.

Tweed D and Vilis T. Geometric relations of eye position and velocity vectors during saccades. *Vision Res* 30: 111–127, 1990a.

Tweed D and Vilis T. The superior colliculus and spatiotemporal translation in the saccadic system. *Neural Networks* 3: 75–86, 1990b.

Uchino Y, Sasaki M, Sato H, Imagawa M, Suwa H, and Isu N. Utriculoocular reflex arc of the cat. *J Neurophysiol* 76: 1896–1903, 1996.

Van Opstal AJ, Hepp K, Suzuki Y, and Henn V. Role of monkey nucleus reticularis tegmenti pontis in the stabilization of Listing's plane. *J Neurosci* 16: 7284–7296, 1996.

Van Rijn LJ and Van Den Berg AV. Binocular eye orientation during fixations: Listing's law extended to induce eye vergence. *Vision Res* 33: 691–708, 1993.

Vilis T. Interactions between the angular and translational components of the VOR. In: *The Vestibulo-Ocular Reflex, Nystagmus and Vertigo*, edited by Sharpe JA and Barber HO. New York: Raven Press, 1993, p. 117–124.

Wade SW and Curthoys IS. The effect of ocular torsional position on perception of the roll-tilt of visual stimuli. *Vision Res* 37: 1071–1078, 1997.

Waitzman DM, Silakov VL, and Cohen B. Central mesencephalic reticular formation (cMRF) neurons discharging before and during eye movements. *J Neurophysiol* 75: 1546–1572, 1996.

Westheimer G. Kinematics of the eye. *J Opt Soc Am* 47: 967–974, 1957.